January 10, 2011

Final Report on Exchange Grant provided by ESF

ORGANISOLAR Activity

"New generation of organic based photovoltaic devices"

# Investigation of photovoltaic properties of pentacene: PTCDI-based organic heterojunctions using organic vapor phase deposition technique

Gamze Saygılı (PhD)

Ege University, Solar Energy Institute,

İzmir/Turkey

Host: Prof. Michael Heuken

Chair of Electromagnetic Theory, RWTH Aachen University,

Aachen/Germany

**02 October-02 December 2010**

**Acknowledgement**

This work would have been impossible without the assistance, support and trust by many people. I would like to express my sincere gratitude the following people/ organizations: Michael Heuken, Holger Kalisch, Sebastian Axmann, Michael Brast, Canan Varlıklı, Sıddık Içli, Ocal Tuna, European Science Foundation (ESF), Organisolar Project.

Best regards,
Gamze Saygili
**E-mail: gsaygl@yahoo.com**

The experimental work has consisted morphology investigations of pentacene and N,N'-Ditridecyl-3,4,9,10-perylenetetracarboxylic diimide (commonly called PTCDI-$C_{13}$) organic semiconductors and organic solar cell (OSC) applications based on these organics. Thin films and device fabrications were performed by using organic vapor phase deposition (OVPD) technique. OVPD has many advantages such as high material utilization efficiency, thickness uniformity in large area, low vacuum operation, high deposition rates, fewer particle and reproducibility compared to vacuum thermal evaporation (VTE).

The goals were:

- To investigate the morphological properties of pentacene and PTCDI-$C_{13}$ by changing of OVPD parameters.
- To optimization of deposited layers in terms of morphology, roughness and thickness
- To investigate photovoltaic properties of pentacene: PTCDI-$C_{13}$

My stay in ITHE-RWTH has been very beneficial; in particular first OSC experiments were done by using OVPD and the morphologies of used organics were studied in detail by atomic force microscopy (AFM) and ellipsometry. I have experience a work activity in an international environment. I would like to thank ESF for the accepted grant. The detailed experimental results will be presented below.

## 1. Introduction

Organic solar cells (OSC) have attracted much attention as a promising choice for unconventional energy source because of their low-cost potential, light weight, mechanical flexibility and ease of processing [1–5].

By using of new materials and improved device architectures, the power conversion efficiency of OPV has significantly enhanced. To date, power conversion efficiencies have reached up to ~5–6% [6-10] for both bilayer and bulk heterojunction OPV and 8.3 % efficiency of OPV certificated by National Renewable Energy Laboratory has reported by Konarka as a record level.

Organic semiconductor devices [OSC, Organic Light Emitting Diodes (OLED), and Organic Thin-Film Transistors (OTFT)] based on either conjugated polymers or small molecules (SM) require different deposition techniques. Organic Vapor Phase Deposition Technique (OVPD), which was invented by S. Forrest et al. at Princeton University in 1995 as an alternative to VTE, one of the deposition techniques for SM [11]. The OVPD system is schematically depicted in fig.1.

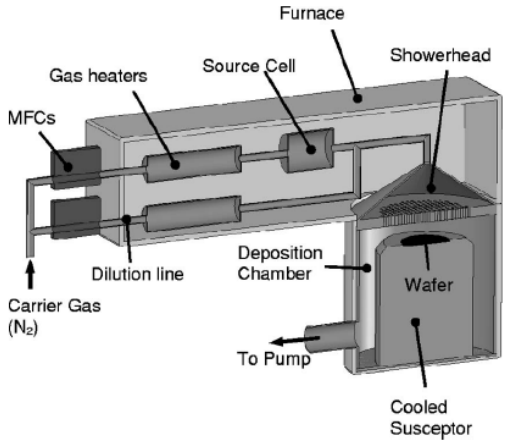


**Figure 1** The schematics of an OVPD tool [12]

In the OVPD system, there are two gas lines: source and dilution line for each source cell. The rate of gas flow is controlled by mass flow controller (MFC). The hot carrier gas passes through the source line and the heated source cell. It transports the material to the cooled substrate in a hot walled chamber (the run-line), where the deposition takes place.

The major focus of this proposal is to use OVPD technique in OSC applications, because of the excellent deposition properties of OVPD. For this purpose, pentacene and PTCDI derivatives can be an attractive choice as an efficient donor/ acceptor combination for excellent charge transport properties and great matching with the solar spectrum, as they showed significant absorption in the complementary part of the visible region [13, 14].

## 2. Experimental procedures

### 2.1 Materials

In this study, pentacene (purity ~ 99.9 %) used as an electron donor material and N, N'-Ditridecyl-3, 4, 9, 10-perylenetetracarboxylic diimide (PTCDI-$C_{13}$) (purity > 99 %) as an electron acceptor material and was purified once before using. All these organic materials were purchased from Sigma-Aldrich. The chemical structures of pentacene and PTCDI-$C_{13}$ and the general structure of the fabricated OSCs are shown in fig. 2 (a-b).

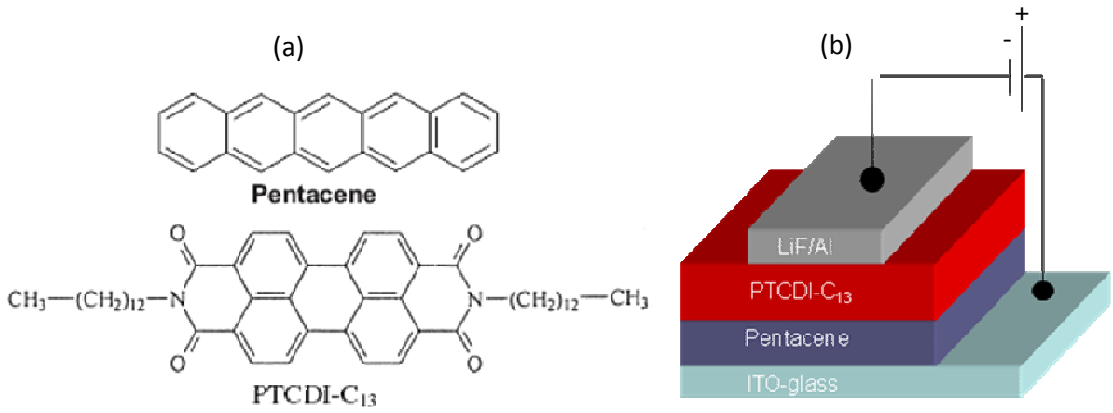


**Figure 2 (a)** The chemical structures of pentacene and PTCDI-$C_{13}$ , **(b)** the general structure of fabricated OSCs.

## 2.2 Film and device fabrications

In order to investigate their morphology, organic materials were deposited on indium tin oxide (ITO)-coated glass substrates (2x2 $cm^2$) and Si-wafer (2x2 $cm^2$). Prior to organic layer deposition, ITO and Si-wafer were cleaned sequentially in ultrasonic baths of detergent, acetone, iso-propanol and deionized water and used pressurized nitrogen gas.

For the OVPD parameters, nitrogen carrier gas at flow rates ranged from 10 to 400 sccm, while the furnace temperature for pentacene was kept at 217 $^{o}$ C and for PTCDI at 325 $^{o}$ C, respectively. The run-line and the showerhead (SH) are heated up sequentially to temperatures around at 330 and 340 $^{o}$ C. The Lauda tool (cryostat) temperature was varied from 20 to 50 $^{o}$ C for cooling block (CB), which is located a few centimeters below the showerhead. The measurements of the substrate temperature are explained detail in the next section. Additionally, the pressure in the deposition chamber was kept at 0.9 mbar and the total gas flow was 550 sccm.

In order to study of surface morphology and to obtain the roughness values of organic layers, organics were deposited on silicon wafer and ITO-glass and Atomic Force

Microscopy (AFM) in tapping mode was used for the measurements. The sizes of observed features were measured by AFM software.

For the device fabrication, pentacene and PTCDI deposited on ITO by OVPD (M-tool), respectively (OVPD parameters are summarized in appendix B). Organic deposited substrate was carried out into other tool (Rudi) for lithium fluoride/aluminum (LiF (~0.5 nm) / Al (~150 nm)) evaporation so that the organics were exposed to air for a short time. Base pressure during the thermal evaporation was ~$10^{-6}$ mbar. The characterization of OSC and measurement set up will be discussed in section 4.

## 2.3 Measurements

### 2.3.1 Substrate Temperature

Substrate temperature is of great importance in terms of size, shape, crystal structure/order and also packaging of molecules. In order to control morphology of thin films and better understand the relationship between the morphology and device performance, the determination of substrate temperature is one of the important parameters.

The substrate temperatures were measured via temperature strips. In principle, the strip contains a small square area. When it reaches the temperature written near the square area for each temperature, the color of the area becomes black. The strips, which were adhered on top of the two ITO-glass substrates, are shown in fig. 3. In this experiment, these samples were kept for a half an hour into the deposition chamber. The Lauda tool (cryostat) temperature was adjusted as 20 $^{o}$ C for the substrate cooling. As can be seen in fig.3, the substrate temperature is between 66- 71$^{o}$ C.

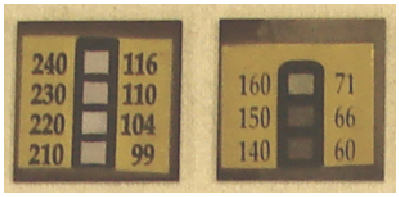


**Figure 3** Image of the strip adhered on top of the ITO-glass substrates. Right side of the each strip shows the temperature in terms of Celsius degree, the left shows Fahrenheit.

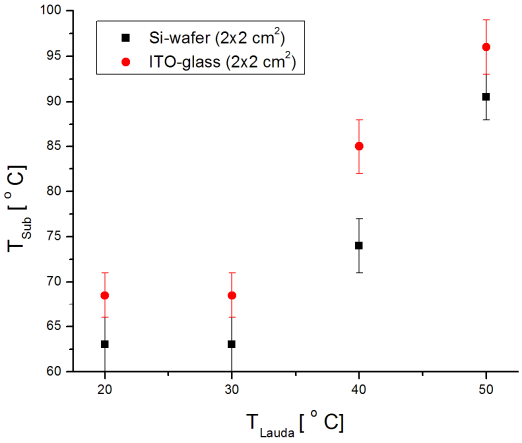


**Figure 4** Determined substrate temperature versus Lauda tool temperature for Si-wafer (2x2 $cm^2$) and ITO-glass (2x2 $cm^2$), $T_{SH}$ = 340 $^{o}$ C.

As seen in fig.4, Si substrate shows lower temperatures compared to those of ITO at the same Lauda tool temperature. The thermal conductivity of substrate is of significant importance for the substrate temperature as well as the morphology of the deposited organics. The direction of the energy flow from the SH (340 $^{o}$ C) to CB (50 $^{o}$ C) is shown in fig.5, while the substrate is between the SH and CB. If the thermal conductivity of substrate is low, there will be large differences between the top and bottom of the substrate due to lower conductivity (in case of the fig.5). Therefore, silicon allows to the more cooling of the substrate than ITO-glass due to its high thermal conductivity (149 W/m K) [15] compared to that of ITO-glass (8.18 W/m K) [16].

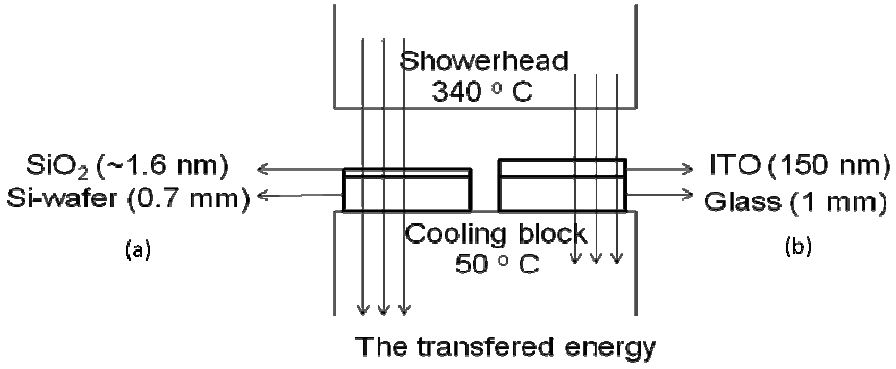


**Figure 5** Images of the mechanism of energy transportation, **(a)** in case of the using $SiO_2$/Si substrate, more energy can transport through the cooling block ($\lambda sio_2$ = 1.4 W/m K, $\lambda si$ = 149 W/m K), **(b)** in case of the using ITO-glass, it is not allowed to efficient cooling due to the low thermal conductivity of ITO-glass (ITO = 8.2 W/m K, $\lambda$ glass = 1.1 W/m K).

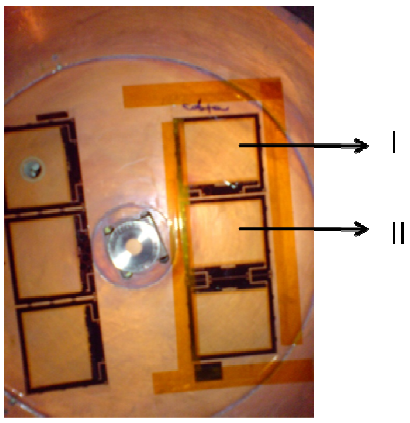


**Figure 6** Substrate positions on the cooling block. One of them was stuck on to the cooling block by the Kapton tape.

The contact between the substrate and the cooling block is another important issue. If the substrate does not contact well with the cooling block, its temperature reaches to higher temperatures than the expected one.

Figure 6 shows the position of ITO (15x5 cm) substrates which were used for the solar cell fabrication. It contains three cells with the 1157 $mm^2$ active area. One of them was stuck by the kapton tape to compare its substrate temperature with that of the substrate without kapton tape. The different temperatures were observed for both substrates especially at higher temperatures of Lauda tool (at 40 and 50 $^o$ C). It is clear

that the substrate does not contact well onto the cooling block. The using kapton tape leads to better interface contact between the substrate and the cooling block resulted in an efficient cooling (fig.7).

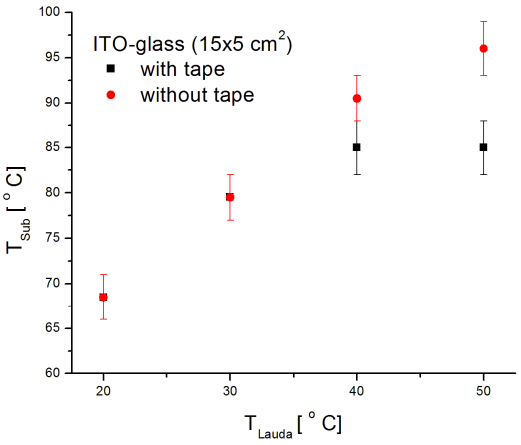


**Figure 7** The substrate temperature versus Lauda tool temperature for ITO-glass (15x5 $cm^2$) with kapton tape and without kapton tape.

Even if the kapton tape is used to fix the substrate onto the cooling block, the substrate temperature is changing at different points of substrate (15x5 $cm^2$). For this purpose, two temperature strips were stuck on per device area, numbered as I* and II* for the substrate with tape and I and II, without tape (fig.6). The Lauda tool (cryostat) temperature was adjusted as 40 $^{o}$ C for the substrate cooling. The samples were kept for a half an hour into the deposition chamber. The substrate temperature ranges were determined for the region I*, II*, I, II as 77-82$^{o}$ C, 82-88$^{o}$ C, 82-88 $^{o}$ C and 88-93 $^{o}$ C, respectively.

For both substrates (with and without kapton tape), middle region showed higher temperature range compared to the edges. It may be explained that the substrates are banding. A big difference forms between the top and bottom of the substrate, while the

showerhead and cooling block temperature are 340 $^{o}$ C and below 50 $^{o}$ C, respectively. The top of the substrate tends to broadened caused by high temperature, whereas the bottom tends to become narrow due to the cooling resulted in a banding of substrate.

## 3. Structural characterization of deposited layers

### 3.1 Morphology studies of pentacene

The Lauda tool temperature was varied between 20 and 50 $^{o}$ C. By changing the gas flow rates, the morphologies of pentacene deposited on ITO and si-wafer were studied. The parameters of OVPD for pentacene depositions are summarized at the appendix A.

#### 3.1.1 Changes of pentacene morphology at 20 $^{o}$ C

In this section, the Lauda tool temperature was kept at 20 $^{o}$ C for each deposition and the effect of the gas flow rates on the morphology were studied. The AFM images of pentacene thin films grown on both ITO and Si-wafer are shown in fig.8.

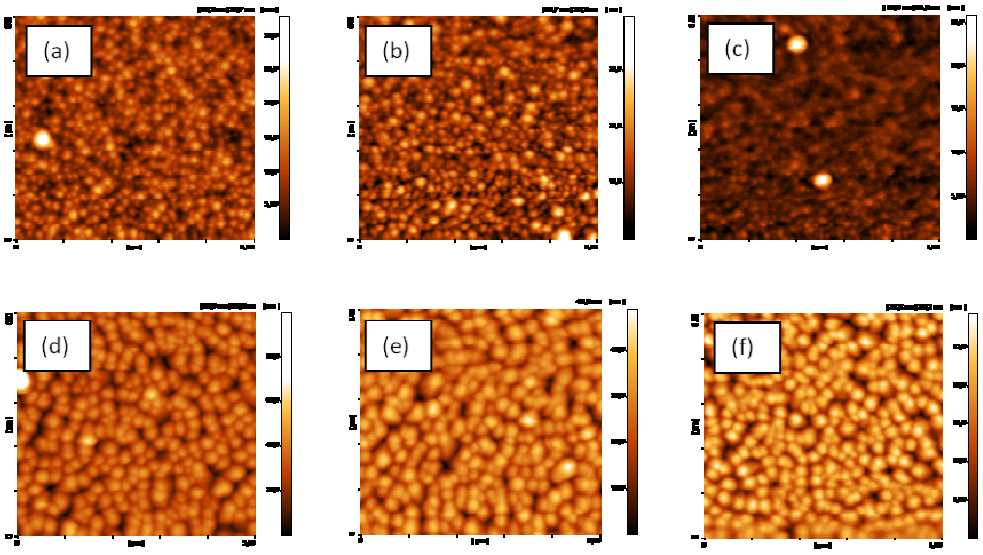


**Figure 8** AFM images of pentacene thin films on ITO, (a) 100 sccm, (b) 200 sccm, (c) 300 sccm, and on silicon, (d) 100 sccm, (e) 200 sccm, (f) 300 sccm.

As seen from the AFM images, pentacene morphologies were grown as small features on both Si and ITO. Pentacene morphology on ITO and on Silicon (at low temperature) shows similarity reported in literature [17, 18].

The roughness values of the deposited pentacene thin films are not comparable as the thin films have different thickness and by changing both gas flow and deposition time. However, for each gas flow rate the roughness of the pentacene film deposited on ITO is lower than that of the silicon substrate.

The size distribution of deposited pentacene on both ITO and si-wafer are shown in Table-1. The grain size was not significantly affected by changing of the gas flow for the same substrate (only ITO or si), even if thin films have different thicknesses. Due to the different properties (roughness, surface energy, thermal conductivity etc.) of the substrates, larger features formed on si-wafer. The lower roughness may lead to the lower diffusion length resulted in larger features. However, there is no significant difference for the grain size of pentacene grown on si and ITO-glass. Pentacene molecules may also stick onto the substrate without finding energy to move due to lower substrate temperature. The formation larger features and lower substrate temperature may cause to the rougher surface in case of using si-wafer.

**Table 1** The summary of the condition of pentacene deposition, morphological results

| Gas Flow (sccm) | Deposition time (s) | Substrate | Roughness (nm) | Grain size (nm) |
|---|---|---|---|---|
| 100 | 3000 | ITO | 6.54 | 150+/-16 |
| 200 | 2000 | ITO | 4.17 | 141+/-14 |
| 300 | 1000 | ITO | 1.97 | 120+/-20 |
| 100 | 3000 | Si | 9.06 | 246+/-39 |
| 200 | 2000 | Si | 6.88 | 261+/-33 |
| 300 | 1000 | Si | 4.99 | 258+/-39 |

### 3.1.2 Changes of pentacene morphology at 30 $^{o}$ C

In this section, the Lauda tool temperature was kept at 30 $^{o}$ C for each deposition and the morphology were studied by changing of the gas flow rates from 10 to 400 sccm. The AFM images of pentacene thin films grown on Si-wafer are shown in fig.9.

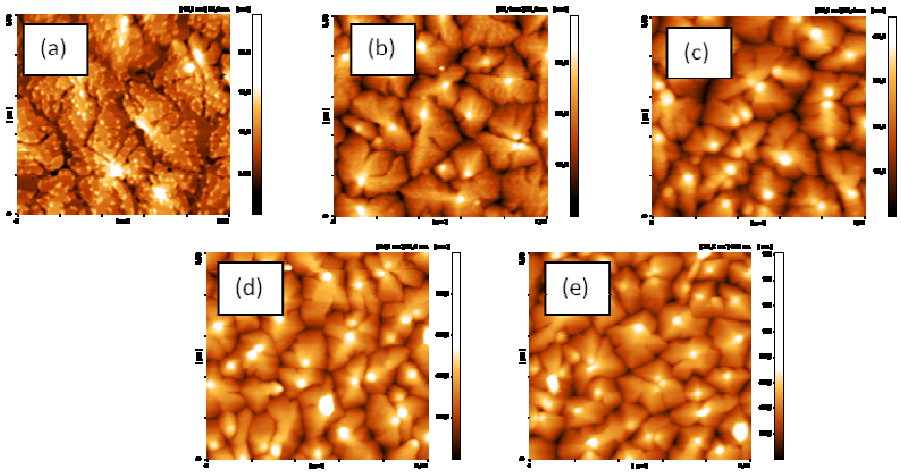


**Figure 9** AFM images of pentacene thin films (a) 10 sccm, (b) 50 sccm, (c) 100 sccm, (d) 200 sccm, (e) 400 sccm.

It can be seen clearly, the morphology of pentacene on si-wafer at 30 $^{o}$ C is quite different from that on si-wafer at 20 $^{o}$ C. This result showed that pentacene morphology is temperature dependent.

A terraced-shaped island of pentacene molecules was obtained by OVPD technique, while the gas flow rate was 10 sccm during the deposition. By increasing both thickness and gas flow, these grains aggregate into a smaller size with the appearance of the pyramid-like.

Roughness is also increasing depending on an increase in the gas flow and thickness. It is difficult to compare the effect of gas flow on thickness and the grain size since the thicknesses of thin films are not in the same range. All data are summarized in Table-2.

**Table 2** The summary of the condition of deposited pentacene on si-wafer, morphological thickness and roughness results before and after annealing.

| Gas Flow (sccm) | Substrate | Roughness (nm) | Roughness after annealing (nm) | Thickness monitored by QCM (nm) | Average grain size (μm) |
|---|---|---|---|---|---|
| 400 | Si | 14.8 | 31.0 | 151 | ≤ 0.5 |
| 200 | Si | 11.3 | 20.0 | 105 | ≤ 0.4 |
| 100 | Si | 7.4 | 9.4 | 67 | ≤ 0.7 |
| 50 | Si | 5.5 | 5.5 | 40 | ≤ 0.7 |
| 10 | Si | 2.6 | 2.7 | 14 | ≤ 1.2 |

The surface morphologies of pentacene deposited on ITO can be seen in fig.10 (a-b-c). Although the substrate temperature was increased, the similar features were observed compared to the morphology of pentacene grown on ITO at 20 $^{o}$ C. However, the size of particles becomes larger at higher cooling temperature (30 $^{o}$ C). All data are summarized in Table-3.

**Table 3** The summary of the condition of deposited pentacene on ITO, morphological, thickness and roughness results before and after annealing.

| Gas Flow (sccm) | Substrate | Roughness (nm) | Roughness after annealing | Thickness monitored by QCM (nm) | Grain size (nm) |
|---|---|---|---|---|---|
| 200 | ITO | 5.0 | 4.2 | 105 | 198+/-26 |
| 50 | ITO | 5.6 | 5.3 | 40 | 190+/-20 |
| 10 | ITO | 8.1 | 10.8 | 14 | 262+/-45 |

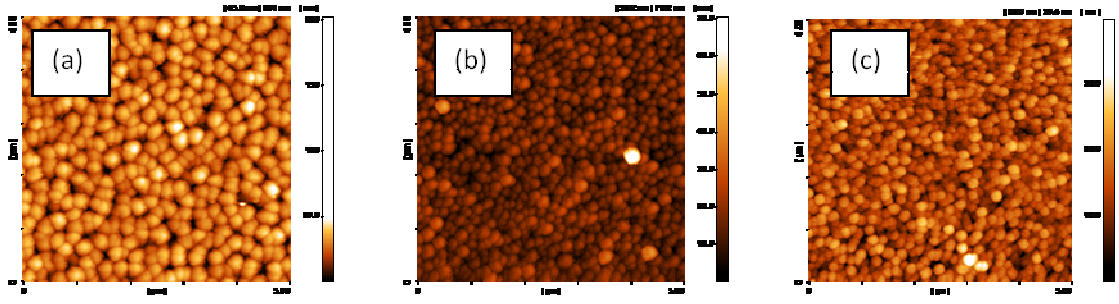


**Figure 10** AFM images of pentacene thin films, (a) 10 sccm, (b) 50 sccm, (c) 200 sccm.

### 3.1.3 Changes of pentacene morphology at 40 $^{o}$ C

In this section, the Lauda tool temperature was kept at 40 $^{o}$ C for each deposition. The morphologies of pentacene molecules were obtained by changing of the gas flow rates from 10 to 400 sccm. The AFM images of pentacene thin films grown on Si-wafer are shown in fig.11.

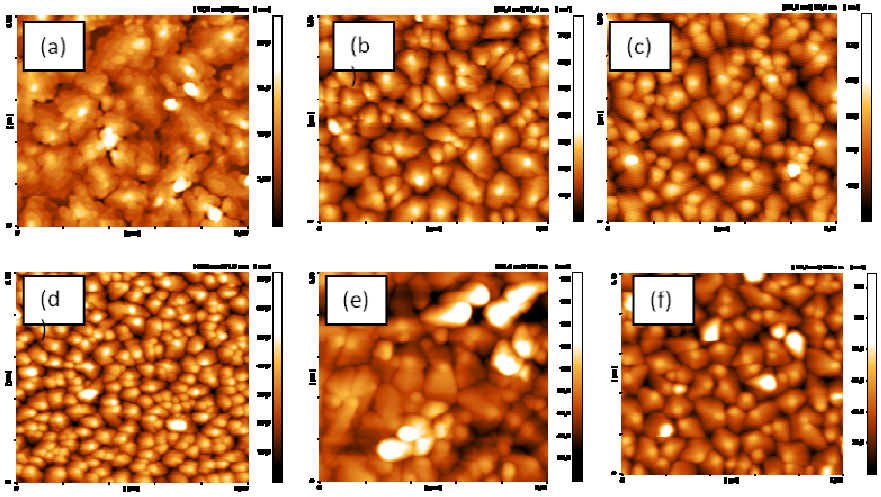


**Figure 11** AFM images of pentacene thin films, (a) 10 sccm, (b) 50 sccm, (c) 100 sccm, (d) 200 sccm, (e) 400 sccm, (f) 400 sccm.

As can be seen in both figures, there is no significant changes in their appearance by increasing of substrate temperature. When the gas flow rate was increased from 10 to 400 sccm, the morphology of pentacene changed from the terraced-shape to the pyramid like structure. The roughness values are increasing by increasing of the gas flow and thickness. The larger grains were obtained compared to those of the samples obtained at 30 $^{o}$ C (summarized in Table-4).

**Table 4** The summary of the condition of pentacene deposition, morphological and thickness results

| Gas Flow (sccm) | Substrate | Roughness (nm) | Roughness after annealing | Thickness monitored by QCM (nm) | Average grain size (μm) |
|---|---|---|---|---|---|
| 400 | Si | 19.5 | 18.2 | 150 | ≤0.8 |
| 200 | Si | 10.2 | 11.8 | 112 | ≤0.9 |
| 100 | Si | 7.3 | 7.9 | 68 | ≤1.1 |
| 50 | Si | 6.8 | 5.8 | 40 | ≤1.5 |
| 10 | Si | 2.9 | 3.8 | 14 | ≤2.6 |

### 3.1.4 Changes of pentacene morphology at 50 $^{o}$ C

In this section, the lauda tool temperature was kept at 50 $^{o}$ C for each deposition. The morphologies of pentacene molecules were obtained by changing of the gas flow rates from 10 to 200 sccm. The AFM images of pentacene thin films grown on Si-wafer and ITO are shown in fig.12 and fig.13.

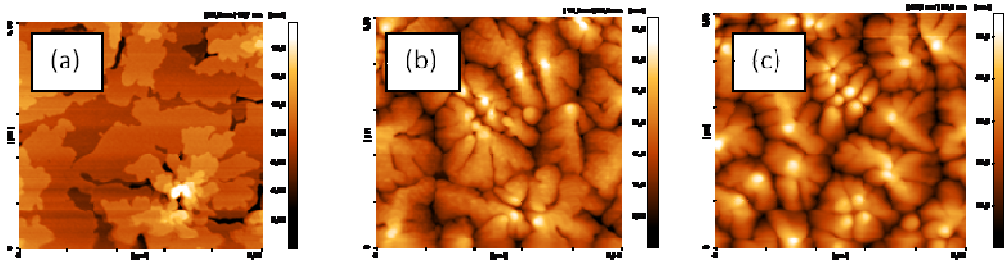


**Figure 12** AFM images of pentacene thin films, (a) 10 sccm, (b) 50 sccm, (c) 200 sccm.

For the deposited pentacene on si-wafer, characteristics pentacene morphologies were observed. By increasing the gas flow rate from 10 to 200 sccm and thickness, the pentacene grains become smaller from 3.51 μm to less than 1 μm (Table-5).

**Table 5** The summary of the condition of pentacene deposition on si-wafer, morphological and thickness results

| Gas Flow (sccm) | Substrate | Roughness (nm) | Roughness after annealing | Thickness monitored by QCM (nm) | Average grain size (μm) |
|---|---|---|---|---|---|
| 200 | Si | 9.0 | 8.9 | 103 | ≤ 1.1 |
| 50 | Si | 5.1 | 5.1 | 38 | ≤ 1.7 |
| 10 | Si | 1.5 | 1.6 | 13 | ≤ 3.5 |

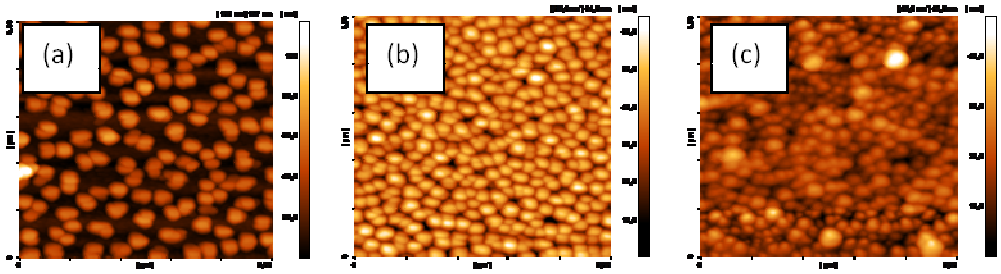


**Figure 13** AFM images of pentacene thin films, (a) 10 sccm, (b) 50 sccm, (c) 200 sccm.

In case of the using ITO, the small features were created with the larger size compared to the obtained morphology at lower cooling temperatures (Table-6). By increasing of the gas flow rate and also increasing of the thickness, the roughness of the thin films is increasing while the sizes of pentacene molecules are not changing linear.

**Table 6** The summary of the condition of pentacene deposition on ITO, morphological and thickness results

| Gas Flow (sccm) | Substrate | Roughness (nm) | Roughness after annealing | Thickness monitored by QCM (nm) | Grain size (nm) |
|---|---|---|---|---|---|
| 200 | ITO | 5.4 | 6.0 | 103 | 316+/-48 |
| 50 | ITO | 8.9 | 13.8 | 38 | 249+/-31 |
| 10 | ITO | 17.7 | 17.9 | 13 | 400+/-45 |

Pentacene shows different morphologies depending on substrate type; In case of the using ITO-glass, the small features were formed, whereas the terraced like and pyramid-shaped structures were observed by changing of gas flow rate for the pentacene grown on si-wafer.

There are several effects cause to the changes of pentacene morphology in case of the using si-wafer and ITO-glass. One is that the used substrates have different thermal conductivity. It is well known that pentacene morphology is temperature dependent. Therefore this may lead to the different morphology for pentacene.

Secondly, the morphology of the pentacene is significantly affected by the surface roughness of the substrate. In principle, the smooth surface facilitates the molecular diffusion of pentacene. Firstly, pentacene molecules diffuse on si-wafer that forms a nucleus where the limited molecules meet together. The next coming molecules not only form a new nucleus but also aggregate into existing islands. However, the rough surface of ITO limits the diffusion of pentacene molecules strongly that may lead to be formed only nucleuses.

At the same cooling temperature, by increasing of the gas flow and the thickness, the roughness of pentacene films are increasing while the grain size are decreasing for the pentacene grown on si-wafer. In case of the using ITO, the roughness of pentacene films is decreasing by increasing of the gas flow and the thickness at the same cooling temperature. This opposite situation can be explained by the differences of surface roughness of substrates. ITO surface is rougher than that of Si-wafer. Pentacene molecules can be deposited disorderly at first due to the rough surface of ITO. By increasing the film thickness, the homogeneous deposition of pentacene improves the rough surface. On the other, due to the smooth surface, pentacene molecules diffuse easily onto silicon and

create larger grains at first. These large grains make the surface rougher (~2.9 nm) compared to the ITO surface (< 1 nm). By increasing the film thickness, the new molecules will be building on large grains with the disordered structures resulted in increase of the roughness by increasing of thickness.

By increasing the cooling temperature from 30 to 50 $^{o}$ C, the grain size of pentacene crystals significantly increases for the same thickness and gas flow rate. Higher temperature increases the diffusion length of molecules that they have a kinetic energy to find stable position. For the roughness values, there is no linear decrease or increase. For instance, when the gas flow rate is 200 sccm, the roughness values are 11.3, 10.2 and 9.0 nm by increasing the cooling temperature from 30 to 40 and 50 $^{o}$ C, respectively. However, when the gas flow rate is 10 sccm, the roughness values are 2.6, 2.9 and 1.6 nm by increasing the cooling temperature from 30 to 40 and 50 $^{o}$ C, respectively.

By increasing the cooling temperature from 30 to 50 $^{o}$ C, the grain size of pentacene crystals and the roughness values significantly increase while the gas flow kept as constant.

### 3.2 Morphology study of PTCDI-C13 grown on ITO and pentacene/ITO

In this section, the lauda tool temperature was kept at 50 $^{o}$ C during the PTCDI deposition (All OVPD parameters are shown at the appendix A-2).

The morphology of PTCDI deposited on ITO can be seen in fig.14. The small and uniform grains were obtained at 250 sccm of gas flow rate. When the thin film was annealed at 100 $^{o}$ C for 5 minutes, the morphology and the roughness of PTCDI thin film did not change significantly.

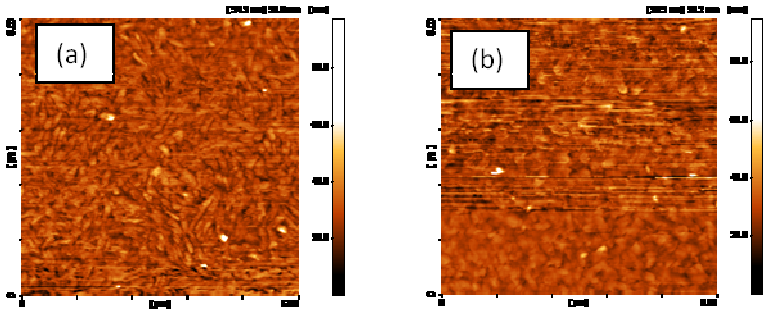


**Figure 14** AFM images of PTCDI thin films deposited at 250 sccm gas flow rate, (a) at room temperature, (b) annealed at 100 $^{o}$C for 5 minutes.

PTCDI was deposited at different gas flow rates and with different thicknesses. However, a few AFM measurements were obtained because of the some difficulties. PTCDI molecules may cause to the very rough surface or may not stick well onto the substrate. As a result, the PTCDI morphology is needed further investigation to obtain accurate roughness values and better morphology.

## 4. Fabrication and characterization organic solar cells (OSCs)

Before the solar cell fabrication, pentacene and PTCDI morphologies were studied. Our aim was to optimize the deposited layers in terms of morphology, thickness. For this purpose, pentacene and PTCDI were deposited on silicon and ITO substrates (2x2 cm$^2$) at different gas flow rates and substrate temperatures while the other OVPD parameters were constant (see appendix A-1 and A-2). Their morphologies, roughness and thickness properties were investigated. However, thickness measurements need to be improved by ellipsometry and PTCDI thin films need to further investigation to obtain better morphology with lower roughness. We have no clear idea for the PTCDI morphology so that we use optimized gas flow rate for the PTCDI (250 sccm, A. Hessel, 2010). Pentacene was deposited at 200 sccm of gas flow rate that gives lower rough film surface

(5 nm). The Lauda tool temperature was kept 50 $^{o}$ C since larger grain size (316 ± 48 nm) of pentacene was obtained compared to the lower temperatures.

Organic solar cells were fabricated with the structure of ITO/pentacene (x nm): PTCDI-$C_{13}$ (y nm)/ LiF (1nm)/ Al (100 nm). The deposition time especially for PTCDI was changed for each cell resulted in a change of thickness. During the fabrication of solar cell, quartz crystal could not be used. Because the quartz crystal should be removed due to the shape of both substrate and mask used for organic deposition. It should be noticed that thickness values of pre-tested with silicon and ITO-glass substrates monitored by QCM were considered for the fabricated OSCs. However, thickness can change even if the same OVPD parameters are used according to the amount of organic in material source cell. Therefore, thicknesses of organic layers were mentioned as estimated thickness for each OSC.

The basic characterizations of fabricated OSCs were done by 2 different methods in our laboratory;

(i) The active area of OSC was illuminated by the bulb light (unknown intensity) of the microscope, the created current by OSC was measured by multimeter (Agilent) (fig 15). The light was switched on/ off while the created current was recorded by software.

(ii) The active area of OSC was illuminated by the bulb light (unknown intensity) of the microscope, their Voc and Jsc values measured by Keithley were manually recorded (fig 15).

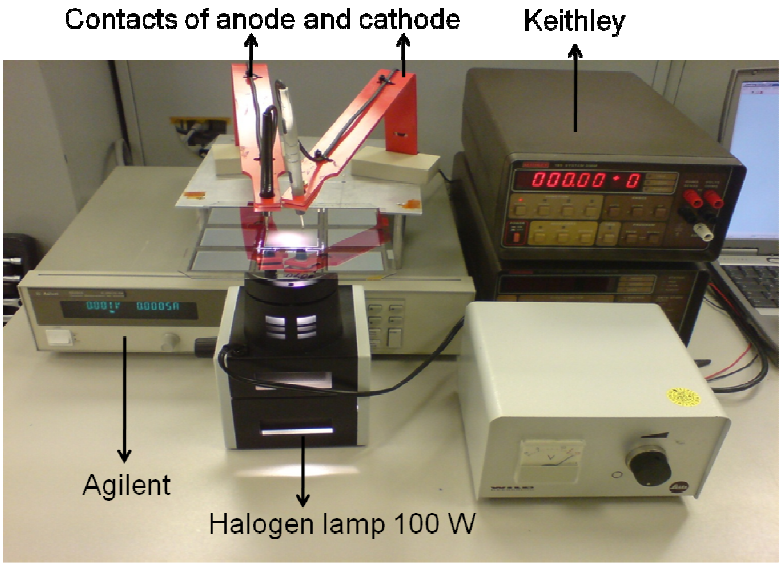


**Figure 15** Basic measurement set up of OSC in our laboratory

In this experiment, the solar cell placed onto the light source, while ITO and Al were connected Agilent voltmeter as an anode and cathode, respectively. Without applying voltage, the light was switched on periodically while the created current by OSC was observed.

The measurement range of Agilent voltmeter was between 0 and 4 Ampere. Since the range is large and the created current in our OSC was generally around micro-ampere, the current signals were obtained with noise. In addition to this, baseline (measured current values were above or below zero while the light was switched off) needed to be adjusted zero for some experimental results. That's why these results are given only to compare current values as an arbitrary unit.

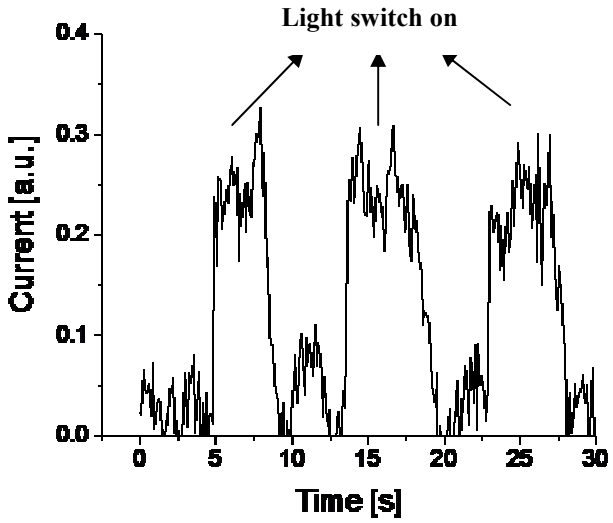


**Figure 16** The Short circuit current vs time under illumination of bulb light. The OSC-A structure is ITO/pentacene (~100 nm)/ PTCDI (~50 nm)/ LiF (~0.5 nm)/Al (100 nm) (recipies 19 and 20- substrate 9914)

Figure 16 shows the created current by one of the OSC-A results as a function of time. As can be seen, when the light was switched on, increased current was observed. In table 7, Voc and Jsc values of OSC-A under illumination of light were summarized.

Although each device was fabricated at the same conditions, they have different Voc and Jsc values. As mentioned previously, the banding of substrate caused to the inhomogeneous substrate temperature. This leads to the different morphology of organic layers that affect strongly the charge transportation.

**Table 7** The open circuit voltage and short circuit current values of the OSC-A with the structure of ITO/pentacene (~100 nm)/ PTCDI (~50 nm)/ LiF (~0.5 nm)/Al (100 nm), measured by Keithley under illumination of bulb light.

| Recipies 19 | Voc (mV) | Jsc (mA/cm$^2$) | Recipies 20 | Voc (mV) | Jsc (mA/cm$^2$) |
|---|---|---|---|---|---|
| Osc1 | 175 | 0.004 | Osc1 | 348 | 0.006 |
| Osc2 | 74 | 0.003 | Osc2 | 3.5 | 0.0002 |
| Osc3 | 100 | 0.0004 | Osc3 | 1.4 | 0.0001 |
| Osc4 | 6 | 0.0003 | Osc4 | 1 | 0.0001 |

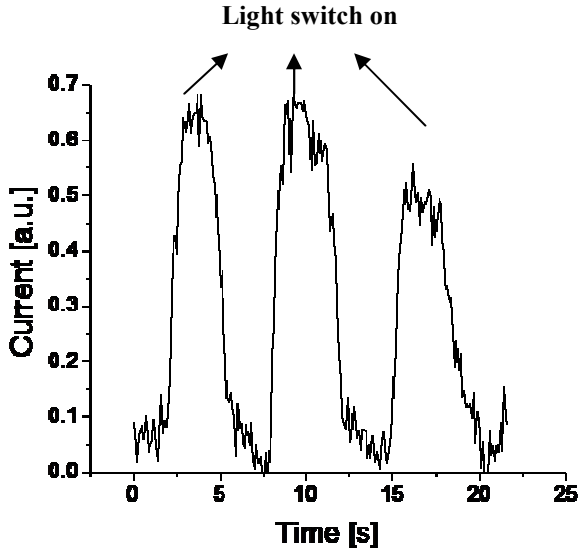


**Figure 17** The Short circuit current of the OSC-B with the structure of ITO/pentacene (~100 nm)/ PTCDI (~84 nm)/ LiF (~0.5 nm)/Al (100 nm) vs time (recipies 21 and 22- substrate 9914).

In case of the increase of PTCDI layer, the Jsc reached up to higher current levels compared to OSC-A (fig.17). Table 8 shows Voc and Jsc values of OSC-B under illumination of the light. The fluctuating was observed between the Voc and Jsc values due to the substrate banding. As can be seen from the Table-8, the solar cells were fabricated at two different substrate temperatures with the same OVPD parameters. But a remarkable change in Voc and Jsc values was not observed.

**Table 8** The open circuit voltage and short circuit current values of the OSC-B with the structure of ITO/pentacene (~100 nm)/ PTCDI (~84 nm)/ LiF (~0.5 nm)/Al (100 nm), measured by Keithley under illumination of bulb light

| Rec 21- Tsubs = 50 ° C | Voc (mV) | Jsc (mA/cm$^2$) | Rec21- Tsub =20 °C | Voc (mV) | Jsc (mA/cm$^2$) |
|---|---|---|---|---|---|
| Osc1 | 0.68 | 0.00004 | Osc6 | 380 | 0.01 |
| Osc2 | 0.28 | 0.00002 | Osc7 | 106 | 0.004 |
| Osc3 | 200 | 0.1 | Osc8 | 17 | 0.0006 |
| Osc4 | 500 | 0.02 | - | - | - |

Several OSC were fabricated with different PTCDI thickness. Similar results were obtained with the result mentioned above. As a result, there is no linear change by changing PTCDI thickness. Obtained $J_{sc}$ values are very low compared to literature. For the pentacene: PTCDI based OSC, $J_{sc}$ was theoretically calculated as 13 mA/ $cm^2$, experimentally reported 8.6 mA/ $cm^2$ [19].

## 5. Conclusion

The first experiments to obtain "working OSCs" by our OVPD system were successfully achieved. We found maximum Voc and Jsc values as 200 mV and 0.1 mA/$cm^2$ for OSC-B3 with the structure of ITO/pentacene (~100 nm)/ PTCDI (~84 nm)/ LiF (~0.5 nm)/Al (100 nm).

We observed that the substrate temperature changes depending on substrate type, size and fixing conditions onto the cooling block. The changes of substrate temperature lead to different film morphology and also significantly affect the device performance.

Organic molecules such as pentacene can package differently depending on substrate type and substrate temperature that gives different morphologies. The morphology affects directly charge mobility in organic layer and also charge transport in a device. Therefore, one should consider the same conditions (especially substrate and order of deposited layers should be the same for investigation of morphology) to investigate the relationship between the morphologic properties of organic layers and OSC performance.

By OVPD technique, we observed reproducible and varied morphologies that are important parameters to obtain an efficient OSC. However, the standard measurement set up will be established to investigate OSCs in terms of efficiency and electrical

characteristics. It will be possible to obtain comparable result with the reported in literature and to improve experimental results for possible publication.

## 6. Our challenges and future plan

Optimization of organic layers in terms of thickness, morphology and roughness need to be improved and further investigation. Beside the optimization thickness, obtaining lower roughness and better morphology, hole and electron mobilities of the organics are of great importance to obtain an efficient OSC. Their mobilities can be investigated by their single layer carrier SCL (space charge limited) diode current-voltage characteristics.

Organics and cathode material should be deposited in a one tool. Because organic layers exposure to air resulted in a degradation of organics and dusts also lead to pin hole in the aluminum layer causing deterioration in device performance. Deposition of pentacene: PTCDI and evaporation of cathode materials in a one tool will be performed in our laboratory while this system will be established and optimized in following days.

To control of the thickness during the deposition of organics is one of the important parameters. New masks should be produced that allow using QCM and control thickness during the organic depositions for OSCs.

The changes in contact between the substrate and the cooling block also affect the substrate temperature, organic morphology and device performance. If there is no reproducibility, it will be difficult to compare obtained results. However, using kapton tape is not a real solution to fix the substrate onto the cooling block. For this purpose, a special sample holder should be produced.

# 7. Appendix

## Appendix A: Parameters of used recipies during the investigation of the surface morphology of organic layers

### *Terminology of OVPD system*

***Furnace1:*** *The heat source of pentacene container.*

***Furnace2:*** *The heat source of PTCDI container.*

***HL1C_Runline:*** *The hot way for pentacene + gas carrier between the furnace1 and deposition chamber.*

***HL2C_Runline:*** *The hot way for PTCDI + gas carrier between the furnace2 and deposition chamber.*

***CCC_Gas_In:*** *Inside of the deposition chamber.*

***SHC_Top and SHC_Bottom:*** *The top and bottom side of the showerhead.*

***DC_Pressure:*** *The pressure of the deposition chamber.*

***F1_Source1_Flow_500:*** *The mass flow controller for the hot carrier gas passed into the pentacene container.*

***F1_Dilution_Flow:*** *The mass flow controller for the hot carrier gas injected to the dilution line.*

***F2_Source_Flow:*** *The mass flow controller for the hot carrier gas passed into the PTCDI container.*

***F2_Dilution_Flow:*** *The mass flow controller for the hot carrier gas injected to the dilution line.*

**A-1:** The parameters of OVPD during the pentacene deposition

| UNIT | TEMPERATURE ($^{o}$C) | Time (s) | Pressure (mbar) | Gas flow (sccm) |
|---|---|---|---|---|
| Material source | 217 | - | - | - |
| HL1C_Run-line | 300 | - | - | - |
| CCC_Gas_In | 340 | - | - | - |
| SH -Top | 340 | - | - | - |
| SH-Bottom | 340 | - | - | - |
| DC_Pressure | - | - | 0.9 | - |
| Total carrier gas flow | - | - | - | 550 |

**A-1-1: The lauda tool temperature was 20 $^{o}$C and pentacene deposited with the gas flow rates at (a) 100sccm, 3000s (b) 200, 2000s and (c) 300 sccm, 1000s, respectively.**

**A-1-2: The lauda tool temperature was 30 $^{o}$C and pentacene deposited with the gas flow rates at (a)10, (b) 50, (c) 100, (d) 200 and (e) 400 sccm, respectively. The deposition time of pentacene was 900s.**

**A-1-3: The lauda tool temperature was 40 $^{o}$C and pentacene deposited with the gas flow rates at (a)10, (b) 50, (c) 100, (d) 200 and (e) 400 sccm, respectively. The deposition time of pentacene was 900s.**

**A-1-4: The lauda tool temperature was 50 $^{o}$C and pentacene deposited with the gas flow rates at (a) 10, (b) 50 and (c) 200, respectively. The deposition time of pentacene was 900s.**

**A-2:** The parameters of OVPD during the PTCDI-$C_{13}$ deposition

**A-2-1 PTCDI on ITO**

| UNIT | TEMPERATURE ($^{o}$ C) | Time (s) | Pressure (mbar) | Gas flow (sccm) |
|---|---|---|---|---|
| Furnace2 | 325 | - | - | - |
| HL2C_Runline | 330 | - | - | - |
| CCC_Gas_In | 340 | - | - | - |
| SHC_Top | 340 | - | - | - |
| SHC_Bottom | 340 | - | - | - |
| Substrate Temp | 50 | | | |
| Deposition time (PTCDI) | - | 2000 | - | - |
| DC_Pressure | - | - | 0.9 | - |
| Total carrier gas flow | - | - | - | 550 |
| F2_Source_Flow | - | - | - | 250 |
| F2_Dilution_Flow | - | - | - | 50 |

**A-2-2 PTCDI on pentacene /ITO**

| UNIT | TEMPERATURE ($^{o}$ C) | Time (s) | Pressure (mbar) | Gas flow (sccm) |
|---|---|---|---|---|
| Furnace1 | 217 | - | - | - |
| Furnace2 | 325 | | | |
| HL1C_Runline | 300 | - | - | - |

| | | | | |
|---|---|---|---|---|
| HL2C_Runline | 330 | - | - | - |
| CCC_Gas_In | 340 | - | - | - |
| SHC_Top | 340 | - | - | - |
| SHC_Bottom | 340 | - | - | - |
| Substrate Temp(pentacene) | 30 | - | - | - |
| Substrate Temp(PTCDI) | 50 | - | - | - |
| Deposition time (pentacene) | - | 900 | - | - |
| Deposition time (PTCDI) | - | 2000 | - | - |
| DC_Pressure | - | - | 0.9 | - |
| Total carrier gas flow | - | - | - | 550 |
| F1_Dilution_Flow | - | - | - | 100 |
| F2_Source_Flow | - | - | - | 250 |
| F2_Dilution_Flow | - | - | - | 50 |

**A-2-2(a) F1_Source1_Flow_500 = 10 sccm**

**A-2-2(b) F1_Source1_Flow_500 = 200 sccm**

## Appendix B: OVPD parameters for the fabrication of OSCs

Constant OVPD parameters for B (1-2-3-4-5)

| **UNIT** | **TEMPERATURE ($^{o}$C)** | **Time (s)** | **Pressure (mbar)** | **Gas flow (sccm)** |
|---|---|---|---|---|
| Furnace1 | 217 | - | - | - |
| Furnace2 | 325 | - | - | - |
| HL1C_Runline | 300 | - | - | - |
| HL2C_Runline | 330 | - | - | - |
| CCC_Gas_In | 340 | - | - | - |
| SHC_Top | 340 | - | - | - |

| | | | | |
|---|---|---|---|---|
| SHC_Bottom | 340 | - | - | - |
| Deposition time (pentacene) | - | 900 | - | - |
| DC_Pressure | - | - | 0.9 | - |
| Total carrier gas flow | - | - | - | 550 |

## B-1 : Recipie 19 and 20

| UNIT | TEMPERATURE ($^{o}$C) | Time (s) | Pressure (mbar) | Gas flow (sccm) |
|---|---|---|---|---|
| Deposition time (pentacene) | - | 900 | - | - |
| Deposition time (PTCDI) | - | 1200 | - | - |
| F1_Source1_Flow_500 | - | - | - | 200 |
| F1_Dilution_Flow | - | - | - | 100 |
| F2_Source_Flow | - | - | - | 250 |
| F2_Dilution_Flow | - | - | - | 50 |

## B-2: Recipie 21 and 22

| UNIT | TEMPERATURE ($^{o}$C) | Time (s) | Pressure (mbar) | Gas flow (sccm) |
|---|---|---|---|---|
| Deposition time (pentacene) | - | 900 | - | - |
| Deposition time (PTCDI) | - | 2000 | - | - |
| F1_Source1_Flow_500 | - | - | - | 200 |
| F1_Dilution_Flow | - | - | - | 100 |
| F2_Source_Flow | - | - | - | 250 |
| F2_Dilution_Flow | - | - | - | 50 |

## B-3: Recipie 23

| UNIT | TEMPERATURE ($^{o}$C) | Time (s) | Pressure (mbar) | Gas flow (sccm) |
|---|---|---|---|---|
| Furnace2 | 335 | - | - | - |

| | | | | |
|---|---|---|---|---|
| HL2C_Runline | 340 | - | - | - |
| Deposition time (pentacene) | - | 900 | - | - |
| Deposition time (PTCDI) | - | 2000 | - | - |
| F1_Source1_Flow_500 | - | - | - | 200 |
| F1_Dilution_Flow | - | - | - | 100 |
| F2_Source_Flow | - | - | - | 100 |
| F2_Dilution_Flow | - | - | - | 50 |

## B-4: Recipie 33

| UNIT | TEMPERATURE ($^{o}$C) | Time (s) | Pressure (mbar) | Gas flow (sccm) |
|---|---|---|---|---|
| Deposition time (pentacene) | - | 900 | - | - |
| Deposition time (PTCDI) | - | 541 | - | - |
| F1_Source1_Flow_500 | - | - | - | 200 |
| F1_Dilution_Flow | - | - | - | 100 |
| F2_Source_Flow | - | - | - | 250 |
| F2_Dilution_Flow | - | - | - | 50 |

## B-5: Recipie 61

| UNIT | TEMPERATURE ($^{o}$C) | Time (s) | Pressure (mbar) | Gas flow (sccm) |
|---|---|---|---|---|
| Deposition time (pentacene) | - | 976 | - | - |
| Deposition time (PTCDI) | - | 2367 | - | - |
| F1_Source1_Flow_500 | - | - | - | 200 |
| F1_Dilution_Flow | - | - | - | 100 |
| F2_Source_Flow | - | - | - | 100 |
| F2_Dilution_Flow | - | - | - | 50 |

## 8. References


[1] C.W. Tang, Two-layer organic photovoltaic cell, Appl. Phys. Lett. 48 (1986) 183–185.
[2]P.Peumans, A.Yakimov, S.R.Forrest, Small molecular weight organic thin film photodetectors ands olarcells, J.Appl.Phys.93(2003)3693–3723.
[3]J.J.M.Halls, C.A.Walsh, N.C.Greenham, E.A.Marseglia, R.H.Friend, S.C. Moratti, A.B.Holmes, Efficient photodiodes from interpenetrating polymer networks, Nature (London) 376(1995)498–500.
[4] S.Yoo, B.Domercq, B.Kippelen, Efficient thin film organic solar cells based on pentacene/C60 heterojunctions, Appl.Phys.Lett.85(2004)5427–5429.
[5] A.K.Pandey, J.M.Nunzi, Efficient flexible and thermally stable pentacene/C60 small molecule based organic solar cells, Appl.Phys.Lett.89(2006)213506 (3 pages).
[6] S.E.Shaheen, C.J.Brabec, N.S.Sariciftci, F.Padinger, T.Fromherz, J.C. Hummelen, 2.5 % efficient organic plastic solar cells, Appl.Phys.Lett.78 (2001) 841–843.
[7] P.Peumans, S.R.Forrest, Very high efficiency double heterostructure copper phthalocyanine/C60 photovoltaic cells, Appl.Phys.Lett.79(2001)126–128.
[8] G.Li, V.Shrotriya, J.S.Huang, Y.Yao, T.Moriarty, K.Emery, Y.Yang, High efficiency solution processable polymer photovoltaic cells by self organization of polymer blends, Nat.Mater.4(2005)864–868.
[9] S.H.Park, A.Roy, S.Beaupr, S.Cho, N.Coates, J.S.Moon, D.Moses, M.Leclerc, K. Lee, A.J.Heeger, Bulk heterojunction solar cells with internal quantum efficiency approaching 100%, Nat.Photon.3(2009)297–302.
[10] H.Y.Chen, J.Hou, S.Zhang, Y.Liang, G.Yang, Y.Yang, L.Yu, Y.Wu, G.Li, Polymer solar cells with enhanced open circuit voltage and efficiency, Nat. Photon. 3(2009)649–653.
[11]P.E. Burrows et al., "Organic vapor phase deposition: a new method for the growth of organic thin films with large optical non- linearities", J. Cryst. Growth 156 (1995) 91-98.
[12] Rolin et al., "Pentacene devices and logic gates fabricated by organic vapor phase deposition", Appl. Phys. Lett. 89, 203502 (2006)
[13] J.M. Nunzi et al., "Pentacene: PTCDI-C13H27 molecular blends efficiently harvest light for solar cell applications", Applied Physics Letters, 89 (2006) 113506.
[14] S.Karak et al., "Improved photovoltaicpropertiesofpentacene/N,N'-Dioctyl-3,4,9,10-perylenedicarboximide-basedorganicheterojunctionswith thermal annealing", Solar Energy Materials & Solar Cells 94 (2010) 836–841.
[15] M. Shamsa et al., Journal of Applied physics 103, 083538 (2008)
[16] T. Nakajima et al. Applied surface science 254 (2007) 884-887
[17] Yong-Sang Kim et al., Solid State Phenomena Vols. 124-126 (2007) pp 451-454
[18] Samy A. El-Daly et al., Journal of photochemistry and photobiology A: Chemistry 137 (2000) 15-19.
[19] J.M.Nunzi et al., Journal of Applied physics 102, 034512 (2007)
[20] S.R. Forrest, "Effects of film morphology and gate dielectric surface preparation on the electrical characteristics of organic vapor phase deposited pentacene thin film transistors
[21] C. Daniel Frisbie et al, J.Phys.Chem.B(2004) 108, 19281
[22]C. Rolin et al., "Growth of pentacene thin films by in-line organic vapor phase deposition", Organic Electronics 11 (2010) 100-108.
[23] J. Puigdollers et al, Thin Solid films, 2009, 517, 6271- 6274
[24] Samy A. El-Daly et al., Journal of photochemistry and photobiology A: Chemistry 137 (2000) 15-19.